

Flux balance analysis of metabolism during growth by osmotic cell expansion and its application to tomato fruits

Sanu Shameer^{1,†} , José G. Vallarino^{2,†}, Alisdair R. Fernie² , R. George Ratcliffe^{1,*}  and Lee J. Sweetlove^{1,*} 

¹Department of Plant Sciences, University of Oxford, Oxford, UK, and

²Max Planck Institute for Molecular Plant Physiology, Potsdam-Golm, Germany

Received 15 August 2019; revised 24 November 2019; accepted 20 December 2019; published online 27 January 2020.

*For correspondence (e-mail lee.sweetlove@plants.ox.ac.uk; george.ratcliffe@plants.ox.ac.uk).

[†]These authors contributed equally to this work.

SUMMARY

Cell expansion is a significant contributor to organ growth and is driven by the accumulation of osmolytes to increase cell turgor pressure. Metabolic modelling has the potential to provide insights into the processes that underpin osmolyte synthesis and transport, but the main computational approach for predicting metabolic network fluxes, flux balance analysis, often uses biomass composition as the main output constraint and ignores potential changes in cell volume. Here we present growth-by-osmotic-expansion flux balance analysis (GrOE-FBA), a framework that accounts for both the metabolic and ionic contributions to the osmotica that drive cell expansion, as well as the synthesis of protein, cell wall and cell membrane components required for cell enlargement. Using GrOE-FBA, the metabolic fluxes in dividing and expanding cells were analysed, and the energetic costs for metabolite biosynthesis and accumulation in the two scenarios were found to be surprisingly similar. The expansion phase of tomato fruit growth was also modelled using a multiphase single-optimization GrOE-FBA model and this approach gave accurate predictions of the major metabolite levels throughout fruit development, as well as revealing a role for transitory starch accumulation in ensuring optimal fruit development.

Keywords: flux modelling, fruit development, cell expansion, *Solanum lycopersicum*.

INTRODUCTION

Flux balance analysis (FBA), a method for predicting and analysing steady-state metabolic fluxes, has been widely applied in the study of plant metabolism (Sweetlove and Ratcliffe, 2011; Nikoloski *et al.*, 2015; Gomes de Oliveira Dal'Molin and Nielsen, 2018). The approach requires a matrix of metabolic reaction stoichiometries and an objective function that represents the optimization target of the biological system (Feist and Palsson, 2010). In simple unicellular microorganisms growing in a nutrient-rich environment, where life-cycle events involve only growth and reproduction, the maximization of flux representing the accumulation of biomass components has proved to be a reasonable objective function (Varma and Palsson, 1994; Feist *et al.*, 2007; Feist and Palsson, 2010). In complex biological systems, however, the accumulation of biomass may not be the primary purpose of every cell type in the organism. For example, the principal metabolic objective of fully expanded source leaves is the biosynthesis of sucrose and amino acids for the rest of the plant (Cheung *et al.*, 2014). Moreover, organ

development in plants typically involves phases of cell differentiation, cell division and cell expansion (Gonzalez *et al.*, 2012), and these are not temporally synchronous, meaning that at different stages of organ development different mechanisms of growth are dominant. Metabolism, being closely related to the demands of the cell, is thus likely to vary between these stages of development (Sweetlove and Ratcliffe, 2011; Nikoloski *et al.*, 2015). The cell expansion stage is responsible for the main increase in organ size and metabolic content in plants, and it is the dominant mechanism when growth is measured during plant phenotyping (Fahlgren *et al.*, 2015; Tardieu *et al.*, 2017). This makes understanding metabolism in expanding cells of great interest and relevance to breeding and crop engineering. In its conventional form FBA does not take account of the changing volume of the cell, indicating the need for a new FBA formulation if this objective is to be achieved.

To provide a biological context, we focused on tomato, *Solanum lycopersicum*, which has an extensive phase of cell expansion during fruit development. This process has

been described in detail at the molecular–biochemical level (Valle *et al.*, 1998; Carrari and Fernie, 2006; Carrari *et al.*, 2006; Legland *et al.*, 2012; Biais *et al.*, 2014), and the available biochemical data can be used to guide the new FBA formulation. Tomato is also an important model for fleshy fruit development and ripening, owing to its agronomic value, ease of cultivation and diploid genetics. FBA has been previously used to model steady-state snapshots of tomato fruit metabolism at different stages of development (Colombié *et al.*, 2015). This was achieved by using time-series metabolomic data sets to constrain metabolite accumulation and degradation rates in a model of primary metabolism. This snapshot approach is informative and captures the accumulation of osmolytes for cell expansion in the form of experimental constraints, but it has some disadvantages. First, accurate predictions of metabolic state, including the accumulation of solutes during cell expansion, can only be made by imposing a large number of experimentally measured constraints. Second, the majority of the flux predictions are a direct consequence of the constraints imposed. For example, the rate of starch degradation observed in the model was the result of a constraint that dictates that starch is consumed at a set rate. Third, because each developmental point is modelled without reference to future needs, the context of the metabolic events at a given time point within the overall development programme is lost. In our previous work on fully expanded source leaves we highlighted a similar issue with modelling day and night metabolism separately, and demonstrated that modelling day and night phases simultaneously as a single-diel FBA problem led to better predictions of leaf metabolism (Cheung *et al.*, 2014). Applying a similar multiphase FBA approach to metabolism during tomato fruit development should therefore improve the usefulness of the computational approach.

In this study, we developed a framework for modelling metabolism in expanding cells using FBA. This approach, growth-by-osmotic-expansion FBA (GrOE-FBA), accounts for the metabolic and ionic contributions to the osmotica that drive cell expansion, as well as the synthesis of protein, cell wall and cell membrane components required for cell enlargement. We show how GrOE-FBA can be used to identify the metabolic network fluxes in expanding cells, highlighting the major metabolic differences between dividing and expanding cells. We also show how GrOE-FBA can be combined with a multiphase single-optimization FBA approach to study plant metabolism during organ development. This approach provided evidence that transitory starch stores are necessary for optimal fruit development, and that prevention of starch accumulation during the early stages of fruit development may result in smaller fruits owing to the reduced phloem uptake rate during later developmental stages, where fruit expansion has been observed to be maximal.

RESULTS

Modelling cell expansion using GrOE-FBA

Cell expansion is driven by the accumulation of osmolytes and the resulting influx of water (Boyer *et al.*, 1985). There are two key equations (see Appendix S1 for the derivation of all the equations) that describe the relationship between the osmotic content of a cell and its volume, and which ultimately allow FBA to be used to model metabolism in expanding cells. First, assuming for convenience that the intracellular solutions behave as ideal solutions, the total osmotic content of a cell at steady state is equal to the product of its osmolarity (C_{cell}) and volume (V_{cell}):

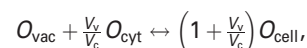
$$\sum n_i m_i = C_{\text{cell}} V_{\text{cell}}, \quad (1)$$

where n_i and m_i are the van't Hoff factor and the number of moles of metabolite i , respectively, in the cell. This equation relates changes in cell volume to changes in osmotic content, and for predicting fluxes it needs to be used in tandem with a second equation that considers the distribution of solutes between the cytosol and the vacuole:

$$\frac{\sum n_j m_j}{\sum n_k m_k} = \frac{V_v}{V_c}, \quad (2)$$

where metabolites j and k are vacuolar and cytosolic, respectively. This equation states that at steady state, the ratio of the osmotic content of the vacuole and cytosol is equal to the ratio of their volumes, V_v and V_c , respectively.

Equations 1 and 2 provide the link between volume and metabolic content at cellular and subcellular levels, and they imply that including a representation of osmotic content in an FBA model should be sufficient to account for volume changes. This was achieved by introducing two pseudo-metabolites in the metabolic network to represent the osmoles associated with the accumulation of osmotically active metabolites/ions in the vacuole and cytosol (O_{vac} and O_{cyt} , respectively; Figure 1a). The pseudo-metabolites take account of the expected differences in the van't Hoff factor by constraining the model so that there can be no net change in the total charge of the vacuole or cytosol. To implement these constraints, two new pseudo-reactions, 'aggregator reactions', were included in the model. The first aggregator reaction:



defined another pseudo-metabolite, O_{cell} , to represent the overall accumulation of cellular osmolytes and constrained the model so that the ratio of accumulation of O_{vac} and O_{cyt} matched V_v/V_c (Equation 2). The second aggregator reaction drains O_{cell} from the system with a flux equal to

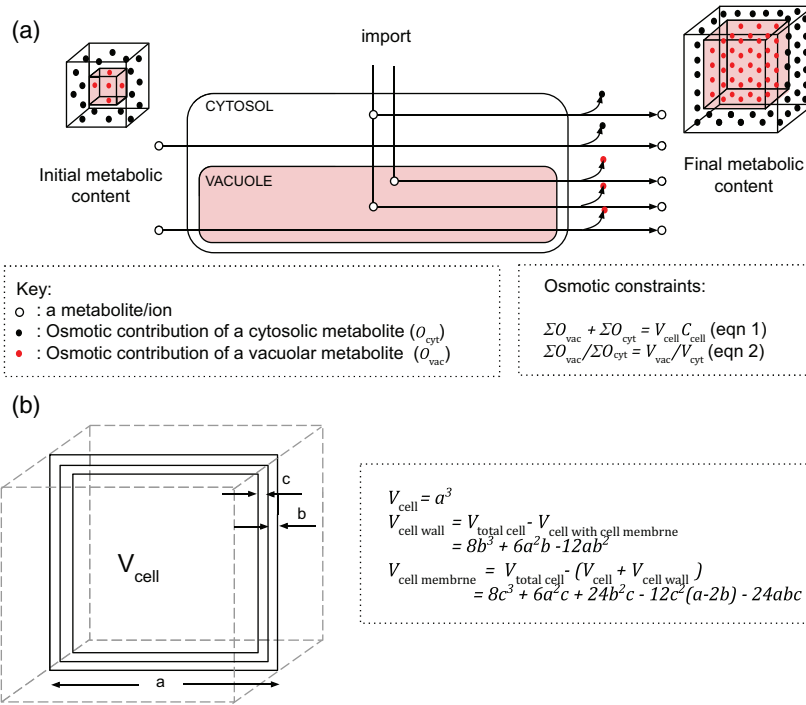


Figure 1. Modelling cell expansion in cube-shaped pericarp cells. (a) Cell expansion is driven by the accumulation of soluble metabolites and ions in the vacuole and cytosol. The accumulation of osmotically active species in the growth-by-osmotic-expansion flux balance analysis (GrOE-FBA) model is accompanied by the accumulation of pseudo-metabolites O_{vac} or O_{cyt} , representing the contribution of the accumulating metabolite/ion to the osmoticum of the vacuole or cytosol, respectively. According to Equation 1, the sum of the vacuolar and cytosolic osmoles is equal to the product of the volume (V_{cell}) and osmolarity (C_{cell}) of the cell. According to Equation 2, the ratio of vacuolar and cytosolic osmoles is equal to the ratio of the vacuolar (V_{vac}) and cytosolic (V_{cyt}) cell fractions. (b) The volumes of the cell wall and cell membrane were calculated by subtracting the remaining parts of the cell from the total cell volume; a , edge length of the cell; b , cell wall thickness; c , cell membrane thickness. Changes in edge length lead to changes in cell volume, but the cell wall and cell membrane thickness are assumed to be constant.

$C_{\text{cell}} V_{\text{cell}}$. This reaction satisfies the steady-state requirement and constrains the model according to Equation 1.

As well as accumulating osmolytes, expanding cells synthesize extra cell wall, cell membrane and proteins to maintain cell functions. Estimates of the additional biomass were obtained by creating a simple geometric representation of a cell, assuming: (i) cells are cubic; (ii) the cell wall is uniformly thick and composed of cellulose only; (iii) the cell membrane is uniformly thick; (iv) the fraction of the total protein content of the cell in the vacuole is negligible; and (v) the cytoplasmic protein concentration is maintained during cell expansion. Based on these assumptions, if V is the volume of the cube-shaped cell, b is the thickness of the cell wall and c is the thickness of the cell membrane (Figure 1b), then the amount of cellulose, phospholipid and protein in the cell can be estimated from the following equations (Appendix S1):

$$\text{moles}_{\text{cellulose}} = \frac{8b^3 + 6b(V_{\text{total cell}})^{2/3} - 12b^2(V_{\text{total cell}})^{1/3}}{MW_{\text{glucose}}} \rho_{\text{cellulose}} \quad (3)$$

$$\begin{aligned} \text{moles}_{\text{phospholipid}} &= \frac{8c^3 + 6c(V_{\text{total cell}})^{2/3} - 24b^2c - 12\{(V_{\text{total cell}})^{1/3} - 2b\} + 24bc(V_{\text{total cell}})^{1/3}}{f_{\text{PM}} MW_{\text{phospholipid}}} \rho_{\text{phospholipid}}, \end{aligned} \quad (4)$$

$$\text{moles}_{\text{protein}} = C_{\text{protein}} V_{\text{cytoplasm}}, \quad (5)$$

where $\text{moles}_{\text{cellulose}}$ is the amount of cellulose in moles, $\rho_{\text{cellulose}}$ is the density of cellulose, MW_{glucose} is the molecular weight of glucose, $\text{moles}_{\text{phospholipid}}$ is the amount of cell membrane phospholipids in moles, f_{PM} is the fraction of the total lipid content found in the plasma membrane, $\rho_{\text{phospholipid}}$ is the density of cell membrane phospholipids, $MW_{\text{phospholipid}}$ is the molecular weight of membrane phospholipid, $\text{moles}_{\text{protein}}$ is the amount of protein in moles (based on how a unit protein is represented in metabolic models), C_{protein} is the molar concentration of protein in the cytoplasm (based on the molar mass of a unit protein as represented in the metabolic model) and $V_{\text{cytoplasm}}$ is the volume of the cytoplasm.

The demand for osmolytes and biomass components required to support a change in cell volume can be

estimated from the difference in the amount of these metabolites for the initial and final cell volumes. For example, the cellulose demand for when a cell changes its volume from V_1 to V_2 can be calculated as follows:

$$\text{flux}_{\text{cellulose}, V_1 \rightarrow V_2} = \frac{\text{moles}_{\text{cellulose}, V_2} - \text{moles}_{\text{cellulose}, V_1}}{\text{time}_{V_1 \rightarrow V_2}},$$

where $\text{moles}_{\text{cellulose}, V_1}$ and $\text{moles}_{\text{cellulose}, V_2}$ are moles of cellulose when the cell has a volume of V_1 and V_2 , respectively, and $\text{time}_{V_1 \rightarrow V_2}$ is the time that the cell takes to change its volume from V_1 to V_2 .

In this manner, by combining previously described osmotic constraints (based on Equations 1 and 2) with biomass constraints (based on Equations 3–5), it is possible to perform FBA while accounting for cell volume.

Validation of the equations used to estimate the change in biomass during cell expansion

The cell wall, lipid and protein contents of tomato pericarp cells during fruit development were determined (Appendix S2) and the results were compared with predictions based on Equations 3–5 (Figure 2). Pericarp cell membrane phospholipid composition was assumed to be composed of phosphatidyl ethanolamine (PE), phosphatidyl choline (PC) and phosphatidic acid (PA), based on published data in cherry tomato (Guclu *et al.*, 1989), and the relative quantities of PE, PC and PA were used to estimate values for $\rho_{\text{phospholipid}}$ and $MW_{\text{phospholipid}}$. The value of f_{PM} was estimated from data published in *Nicotiana tabacum* (tobacco) leaves (Cacas *et al.*, 2016) and was assumed to be constant throughout fruit development. Values of other parameters required in the equations were collected from published data or were measured experimentally (Table S1).

Figure 2 shows that Equations 3–5 generated a good match to experimentally measured values for tomato fruit. The slight underestimation of fruit cellulose content is likely to arise from the assumption of the cells being geometric cubes with a constant cell wall thickness, which does not account for increased cell wall thickness around the corners of the cell (Legland *et al.*, 2012). Thus, a simple geometric model can be used to predict increases in cellulose, phospholipid and protein content during cell expansion, and this allows these major biomass outflows from the metabolic network to be estimated, avoiding the need for direct measurements.

Application of GrOE-FBA to expanding tomato cells

Due to the energy cost of synthesising cellular macromolecules, such as proteins, lipids and carbohydrates (Schwender and Hay, 2012), it is generally assumed that the synthesis of new cells is more expensive than expanding existing cells (Taiz, 1992; Lynch, 2019). Even during cell expansion, however, new macromolecules need to be

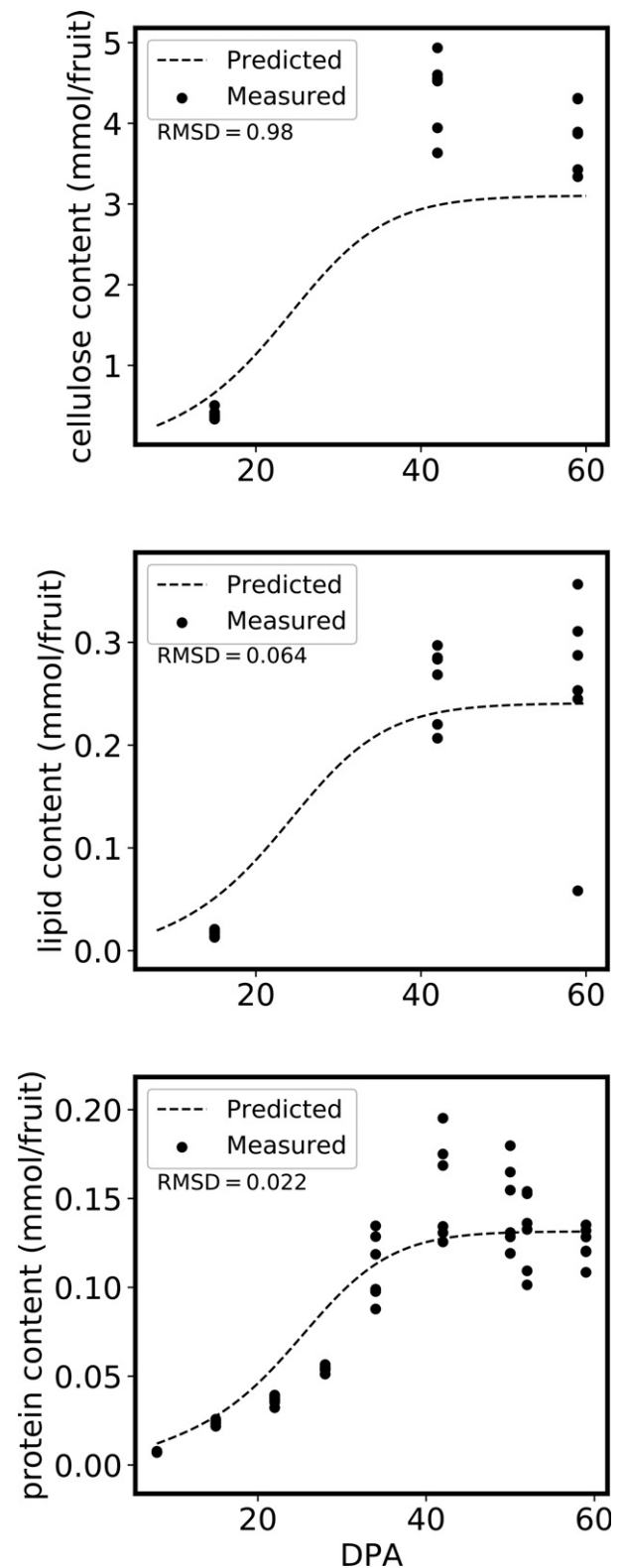


Figure 2. Cellulose, lipid and protein contents of *Solanum lycopersicum* (tomato) pericarp cells. The predicted curves are based on Equations 3–5 for cellulose, membrane phospholipid and protein content, respectively.

produced and the synthesis and accumulation of osmolytes to drive cell expansion also represents a significant cost. The GrOE-FBA framework allows the costs of cell expansion to be computed and the result can be compared with the costs of cell division computed using conventional FBA with a biomass objective. To do this, we modelled rapidly dividing tomato pericarp cells in culture using existing data (Rontein *et al.*, 2002) and compared the resulting model with one of rapidly expanding pericarp cells in tomato fruit. Both models were constructed using a minor updated version (PlantCoreMetabolism_v1_2) of our previously published core stoichiometric model of primary plant metabolism (Shameer *et al.*, 2018). Given the focus on tomato, the model contains tomato gene-to-reaction associations, although these were not used in this study. The dividing cell model was provided with the nutrients present in the cell culture medium: glucose as the sole carbon source, as well as ammonium, oxygen, phosphate and sulphate. The expanding cell model was provided with sugars and amino acids in the same relative proportions as

reported for tomato plant phloem sap (Walker and Ho, 1977a; Valle *et al.*, 1998), as well as oxygen, phosphate and sulphate. The same objective function of minimization of the sum of fluxes was applied to both models. Experimental data were used to constrain the rate of biomass production in the dividing cell model to 2 mg dry weight (DW) $\text{mL}^{-1} \text{day}^{-1}$, which was the fastest rate reported in the Rontein *et al.* (2002) study. The rate of cell expansion in the expanding cell model was set to that of fruit at 26 days post anthesis (DPA), where the fastest rate of fruit growth was observed (Beauvoit *et al.*, 2014). The initial exploration of the expanding cell model included an additional component to the objective function: to maximize the organic solute content while satisfying the osmotic constraint (see subsequent explanations and discussions).

Figure 3 summarizes the results of this comparison for equivalent numbers of cells, and the complete list of predicted fluxes is provided in Appendix S3. Comparison of the metabolic fluxes in the two models revealed that dividing cells have higher fluxes of cellulose, protein, starch

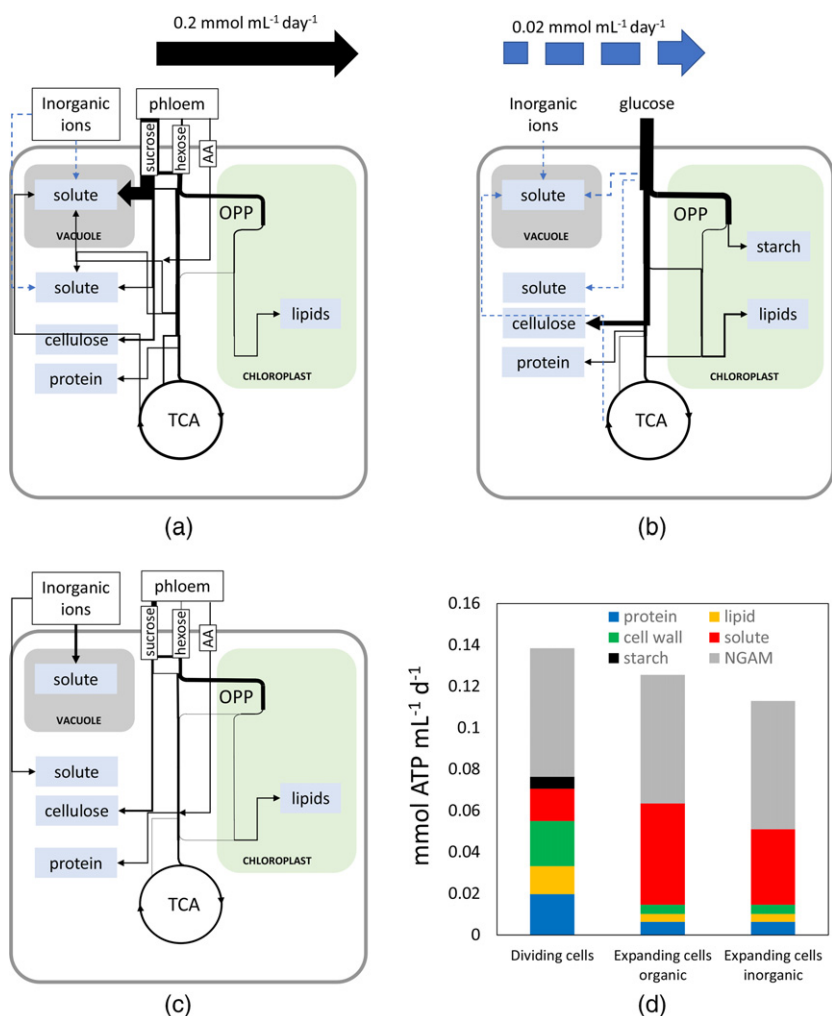


Figure 3. Flux prediction in expanding and dividing *Solanum lycopersicum* (tomato) cells using growth-by-osmotic-expansion flux balance analysis (GrOE-FBA). Predicted metabolic fluxes in: (a) expanding cells accumulating only organic solutes; (b) dividing cells; and (c) expanding cells accumulating only inorganic solutes. Organic and inorganic fluxes are represented as mmol C per ml cellular volume per day and mmol per ml cellular volume per day, respectively, with the thickness of the lines scaled to match the fluxes. Values of all the predicted fluxes are given in Appendix S3. (d) ATP budgets for solute accumulation and for the biosynthesis of protein, lipid, cell wall and starch, deduced from the three predicted flux maps. AA, amino acids; OPP, oxidative pentose phosphate pathway; TCA, tricarboxylic acid cycle.

and lipid biosynthesis, as expected, whereas the expanding cells accumulated significantly more organic solutes, both in the vacuole and cytosol (Figure 3a,b). This accumulation of organic solutes in the expanding cell model increased the carbon demand of the model, and somewhat surprisingly, the overall rate of glucose consumption was higher in the expanding cell model ($2.26 \text{ mg ml}^{-1} \text{ day}^{-1}$) than in the dividing cell model ($1.43 \text{ mg ml}^{-1} \text{ day}^{-1}$). The flux maps (Figure 3a,b) reveal that a substantial proportion of this additional carbon (68% of carbon taken up by the cell) was transported into the vacuole to satisfy the osmotic requirement for cell expansion. But it is also apparent that there were high fluxes of glycolysis, and an even higher tricarboxylic acid (TCA) cycle flux, relative to the dividing cell model, suggesting that the energy demand of cell expansion is comparable with that of cell division. To provide a more precise quantitative comparison of energy costs, we constructed an energy budget for the two systems by collating all the fluxes in the models that required ATP consumption or led to ATP production (Figure 3d). The total ATP demand of the expanding cells was $0.13 \text{ mmol ATP ml}^{-1} \text{ day}^{-1}$ and that of the dividing cells was $0.14 \text{ mmol ATP ml}^{-1} \text{ day}^{-1}$. This showed that indeed both models have very similar energy demands. Tomato fruit development from 13.1 to 43.7 DPA (with mature green fruits observed at 42 DPA) is mainly the result of the expansion of existing cells, and from the breakdown of energy expenditure (Figure 3d) it is apparent that although the expanding cell model devoted considerably less ATP to the synthesis of protein, lipid and cell wall (12% compared with 44% in dividing cells), this was offset by a large increase in the cost of solute biosynthesis and accumulation, which represented 39% of the ATP budget in the expanding cell model compared with only 11% in dividing cells (Figure 3d).

Given that the maximization of organic solute was a component of the objective function of the expanding cell model, the very high rate of accumulation of glucose to satisfy the osmotic constraint may be a feature of how we set up the model. Although it is known that fruit cells contain high quantities of hexose sugars (Biais *et al.*, 2014), it is likely that inorganic solutes contribute to the osmotic balance and this would affect the total energy cost of osmolyte production and accumulation. To explore this we removed the objective for the maximization of organic solute and just used the minimization of the sum of fluxes as the sole objective, as in the dividing cell model. This led to a significantly lower rate of carbon consumption in the expanding cells ($0.63 \text{ mg C ml}^{-1} \text{ day}^{-1}$), but the overall ATP demand remained comparable with that of the previous model ($0.11 \text{ mmol ATP ml}^{-1} \text{ day}^{-1}$). The predicted flux distribution (Figure 3c) revealed that the model was exclusively using inorganic ions to satisfy the osmotic constraints.

In reality expanding cells are expected to accumulate both organic and inorganic solutes to facilitate cell expansion, so the predicted energy demand of the expanding and dividing cells are comparable. These results demonstrate that cell expansion is not necessarily a cheap option for plant growth, as previously argued (Taiz, 1992).

Many similarities between the three systems (dividing cells, expanding cells accumulating organic solute and expanding cells accumulating solely inorganic solute) were apparent. For example, in each system, more than 75% of the ATP demand was met by mitochondrial ATP synthesis (75, 73 and 78%, respectively) and non-growth-associated maintenance (NGAM) was found to be a significant energetic drain (45, 49 and 55% of the total ATP demands, respectively). The second largest energetic demand was the ATP cost of maintaining the plasma membrane proton gradient (PM-ATPase) during nutrient uptake (18, 23 and 29% of the total ATP demands, respectively). Although the basis for NGAM was identical in the three models, the PM-ATPase flux was dependent on the carbon demands of the model. As a result, the energy demand of the system is significantly influenced by the carbon demand for biosynthesis. Note that NGAM was calculated based on an assumed 3:1 ratio of ATP:NADPH expenditure on maintenance (Cheung *et al.*, 2013), but the general conclusion about the comparative overall ATP expenditure in dividing versus expanding cells is not altered if different maintenance ATP:NADPH ratios are used (Figure S1).

A multiphase metabolic model of primary metabolism in developing tomato fruit

To investigate the changing metabolic requirements for growth by cell expansion during organ development, pericarp metabolism was modelled using GroE-FBA in the expansion and ripening stages of developing tomato fruit by dividing the time course from 8 DPA to red ripe stage (59 DPA) into 10 developmental substages. Ten copies of PlantCoreMetabolism_v1_2, each representing one of these substages, were combined to generate a 10-phase constraint-based model of primary metabolism in tomato pericarp cells. To allow for the accumulation and use of sugars (glucose, fructose and sucrose), amino acids (including γ -aminobutyric acid, GABA) and organic acids (malate and citrate) in each phase, reactions transferring metabolites and ions from one phase to the next, called 'linker reactions', were added to the cytosol and the vacuole of the model. Similarly, the transfer of starch from one phase to the next (allowing for the accumulation and use of starch) was enabled via linker reactions in the plastid. The linker reactions and the multiphase nature of the model ensure that metabolism in each stage of fruit development depends not only on metabolism in the previous

developmental stages but is also influenced by that of future developmental stages. Each phase in the multiphase model also had access to the xylem and the phloem, and was subjected to biomass requirements. A full schematic representation of the model is presented in Figure 4.

The initial metabolite content of the fruit pericarp at 8 DPA was established by adding source reactions (reactions that represent the import of metabolites from outside the modelled system) for sucrose, fructose, glucose, amino acids, GABA, organic acids and starch to the first phase of the model. The flux through these source reactions was constrained using the experimentally determined soluble metabolite content of 8-DPA fruits (Appendix S2). The soluble metabolite content of red ripe tomato fruits (59 DPA; Appendix S2) was used to constrain the relative proportions of the soluble metabolites in the final model phase of the model by introducing appropriately constrained sink reactions. Previously published data on vacuolar pH during fruit development in cherry tomatoes (Rolin *et al.*, 2000) was used to set the vacuolar pH for the 10 phases and thus the abundance of the different metabolite charge states for each phase. A data-based constraint was also applied for the maximal rate of uptake of nutrients into the fruit from the phloem (see Experimental procedures). The multiphase developing fruit model was solved as a single parsimonious FBA (pFBA) problem, an approach similar to previously published multiphase (Cheung *et al.*, 2014; Gomes de Oliveira Dal'Molin *et al.*, 2015; Shameer *et al.*, 2018) and multi-tissue (Grafahrend-Belau *et al.*, 2013; Gomes de Oliveira Dal'Molin *et al.*, 2015; Scheunemann *et al.*, 2018; Shaw and Cheung, 2018) constraint-based models, with the maximization of fruit soluble metabolite content as the objective. Fruit content and composition is key in increasing yield in tomato cultivation, and hence the maximization of flux through the reaction representing the accumulation of soluble

metabolites in ripe tomatoes was deemed an apt objective function for the model. NGAM, nutrient uptake from the phloem and the osmotic constraints based on Equations 1 and 2 were implemented as described in the Experimental procedures.

A multiphase developing tomato fruit model predicts realistic final fruit metabolite content

Figure 5 depicts the influence of the various constraints on the predictions of the multiphase developing fruit model. Optimal flux distributions of the model without the osmotic and biomass constraints to describe cell expansion and with no upper limit on phloem uptake rates predicted unrealistically high fruit organic solute content (approx. 5000 mOsmol per fruit; Figure 5 upper left). The introduction of osmotic constraints on the system greatly reduced the final fruit organic solute content to 24.5 mOsmol per fruit (Figure 5 upper right). This value was just 7.5% lower than the measured value (26.5 mOsmol per fruit). The imposition of biomass demand fluxes did not affect the predicted ripe fruit organic content, although it did cause small variations in predicted fruit content during the early stages of fruit expansion (Figure 5 lower right). Limiting the phloem uptake rate had no effect on the predicted organic content of ripe fruits, but it did reveal a requirement for a transitory carbohydrate store in expanding fruits (Figure 5 lower left). The maximum level of starch that was predicted to accumulate was 8.3 mmol hexose equivalents per fruit, corresponding to 1495 mg per fruit. This is 2.8 times the value of 530 mmol hexose equivalents per fruit reported in an experimental study (Petreikov *et al.*, 2009).

In order to understand the factors driving metabolism during fruit development, predicted fruit metabolic content during development was analysed (Table 1). From Table 1 it can be seen that the soluble organic content contributes the most quantitatively significant fraction of fruit content,

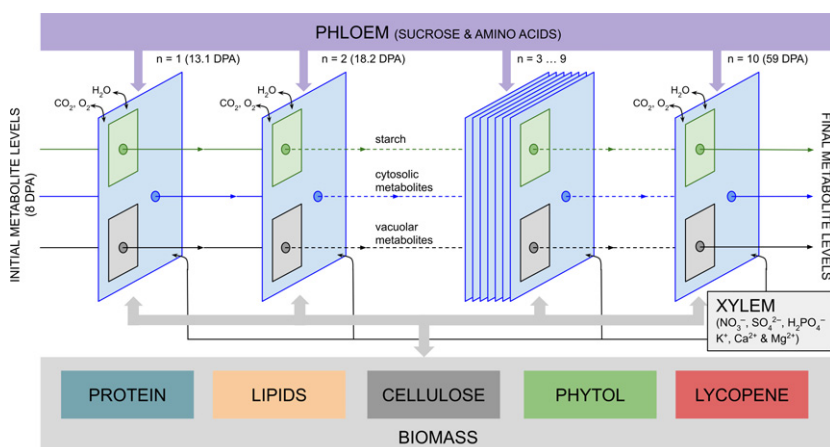


Figure 4. Schematic representation of the multiphase model of *Solanum lycopersicum* (tomato) fruit development. Fruit development from 8 days post anthesis (DPA) to 59 DPA was divided into 10 phases. Each phase has access to the indicated nutrients from the mother plant via xylem and phloem and is subject to biomass demands. The accumulation of certain metabolites and ions was permitted in each phase, facilitated in the model by 'linker reactions' that allow the accumulated metabolites/ions to be passed to the next phase.

particularly during the later stages of fruit development. The optimal flux distribution and a fully constrained version of the multiphase model are available in Appendixes S3 and S4, respectively.

Comparing model predictions with experimental measurements

Figure 6 compares the fruit content of selected metabolites predicted by GrOE-FBA with the experimentally determined values. The complete data set for 22 solutes is provided in Figure S2. The model was capable of making accurate predictions for glucose, fructose, glutamine and glutamate, despite being free to choose which metabolites it accumulated to satisfy the osmotic constraint. These four metabolites formed 88.6% of organic osmolytes in the pericarp cells and their accurate prediction by the osmotically constrained model suggests that their pattern of accumulation in developing tomato fruit represents an efficient way to drive osmotic expansion. Some other metabolite levels, including those of malate and citrate, were predicted with reasonable accuracy during the later stages of fruit development, whereas for others, including sucrose and GABA, it was not possible to predict the observed pattern of accumulation. This suggests that the accumulation of these

metabolites is not primarily driven osmotically and that other aspects of fruit physiology may drive their accumulation during fruit development. For example, factors such as insect resistance, texture and flavour all have an impact on determining fruit composition during development (Tohge *et al.*, 2014; Cohen *et al.*, 2014; Takayama and Ezura, 2015). Translating these factors into constraints for a metabolic model would be challenging, as the measured content of some of the poorly predicted amino acids (aspartate and serine) fell within the FVA ranges of the model (Figure S2), but applying extra constraints to the system may improve the predictive performance of the model.

A transitory carbohydrate store is required when phloem nutrient uptake is limited

If nutrient influx from the phloem was unlimited, then the nutrient requirement for fruit development was predicted to peak in phases 4 and 5 (23.3–33.5 DPA; Figure 7a). In contrast, when an upper bound on phloem uptake (Figure 7b) was imposed, based on experimental data, the model predicted the need for transitory carbohydrate storage (Figure 7d), which is a well-documented behaviour of tomato fruits (Ho and Hewitt, 1986; Gillaspay *et al.*, 1993). When phloem uptake rate limits were removed from the

Figure 5. Impact of model constraints on the predicted metabolite contents of developing *Solanum lycopersicum* (tomato) fruit. The charts show the sequential effect on the predicted metabolite contents of adding osmotic, biomass and phloem uptake constraints to the model. In the absence of these constraints the predicted total metabolite content greatly exceeded the expected value, whereas after applying the constraints there was close agreement between the measured and predicted values. AA, amino acids; OA, organic acids; SUG, sugars (glucose, fructose and sucrose).

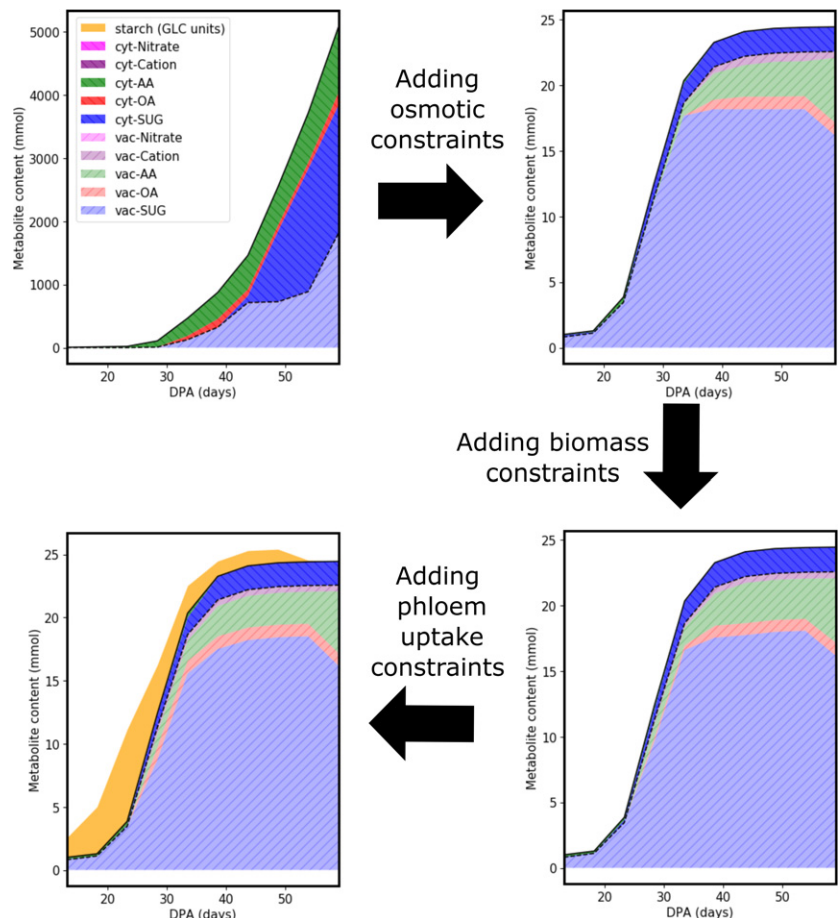


Table 1 Organic content of *Solanum lycopersicum* (tomato) fruits predicted by the multiphase developing fruit model

Phase (DPA)	Fruit content (% fruit DW)					Fruit DW (mg)
	Cellulose	Phospholipids	Protein	Starch	Organic solutes	
8–13.1	9.49	2.81	1.1	27.6	59.0	927.6
13.1–18.2	8.04	2.39	0.91	34.8	53.9	1989
18.2–23.3	6.35	1.88	0.72	31.0	60.1	4104
23.3–28.4	7.45	2.21	0.87	13.4	76.1	4811
28.4–33.5	8.21	2.44	0.97	6.20	82.2	5207
33.5–38.6	8.33	2.47	0.99	2.92	85.3	5587
38.6–43.7	8.15	2.42	0.97	2.74	85.7	5930
43.7–48.9	8.33	2.47	0.99	2.35	85.9	5869
48.9–54.0	8.78	2.61	1.04	0.27	87.3	5562

model there was no accumulation of starch (Figure 7c), suggesting that the accumulation of starch was associated with phloem influx limits and metabolic demand. Moreover, preventing the accumulation of starch caused a 40% drop in the organic content of the fruit, demonstrating the significance of transitory starch storage in developing tomato fruits.

DISCUSSION

GrOE-FBA: proof of concept in the comparison of expanding and dividing cells

GrOE-FBA was developed to predict metabolic network fluxes in cells undergoing osmotically driven cell expansion. As a proof of concept, GrOE-FBA was used to highlight the differences between metabolism in dividing and expanding cells, and the analysis led to the conclusion that cell expansion does not necessarily put a smaller requirement on cellular resources than cell division. Although it is not surprising that differences existed between metabolism in dividing and expanding cells, quantitative network-level comparisons have not been made before. The two systems chosen here for comparison were dividing cells in heterotrophic cell suspension cultures and expanding cells in developing tomato fruits. A more appropriate comparison would be to model metabolism during the very early phase of tomato fruit development, when cell division dominates, and then again for the later phases, when expansion dominates. There is very little biochemical data to constrain such a cell division model, however, because of the very small size of the young plant organs in the cell division phase. Even so, the marked difference in the predicted metabolic fluxes of dividing and expanding cells (Figure 3) implies that conventional FBA studies on plant tissues, such as growing leaves (Yuan *et al.*, 2016; Shaw and Cheung, 2018) and roots (Grafahrend-Belau *et al.*, 2013; Shaw and Cheung, 2018), need careful interpretation, even if they include experimental metabolite

constraints that would indirectly account for the generation of osmotic pressure for cell expansion.

GrOE-FBA: application to tomato fruit development

The GrOE-FBA approach was combined with multiphase modelling to analyse metabolism in developing tomato fruit. The approach required minimal constraints: a knowledge of cell volume changes during expansion, an estimate of the volume ratio of vacuole to cytosol, and an estimate of protein concentration (C_{protein} , Equation 5). Using these constraints, it was possible to make surprisingly accurate predictions about the accumulation of biomass components and the principal osmotic metabolites that drive cell expansion in tomato fruit (Figures 5 and 6). The same approach could be applied to the growth of other organs such as leaves and roots.

Previous modelling studies taking into account cell expansion and metabolism were based on an analysis of enzyme kinetics and were capable of exploring only limited aspects of metabolism because of the difficulty of gathering or estimating large numbers of kinetic parameters (Beauvoit *et al.*, 2014). Previous work using FBA modelling to analyse metabolism in developing tomato fruits used separate models for each stage of development (Colombié *et al.*, 2015). Such highly constrained models can provide answers to the question ‘What is happening?’ but cannot answer the question ‘Why is this happening?’. For example, with this approach it has been shown that the breakdown of transitory starch is the underlying cause of the respiratory climacteric in tomato fruit (Colombié *et al.*, 2017), but it was not possible to explain the purpose of the transitory accumulation of starch. This is because starch accumulation and degradation were constraints of the model and not predictions. In contrast, starch accumulation and degradation in the multiphase GrOE-FBA model are system-level predictions that depend on the metabolic demand on the system and the availability of nutrients from the phloem, throughout development.

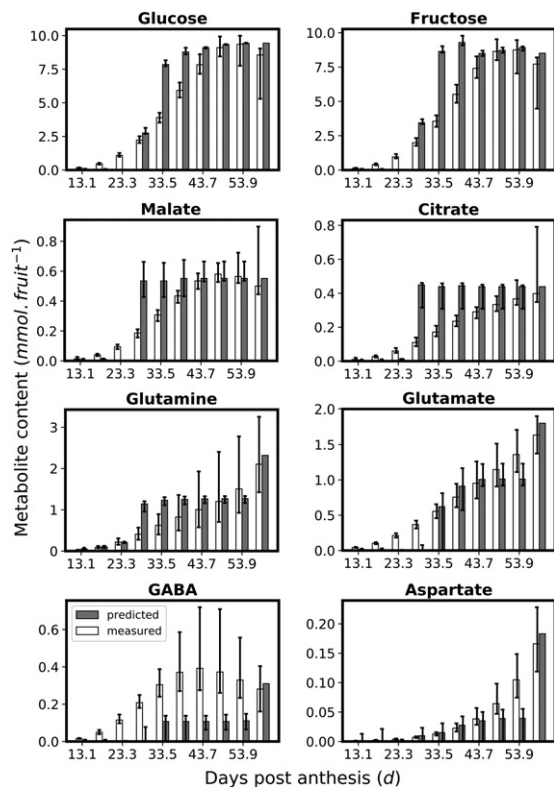


Figure 6. Comparison of predicted and measured metabolite contents in developing *Solanum lycopersicum* (tomato) fruit. The predicted metabolite contents are in good agreement (glucose, fructose, glutamine, glutamate), partial agreement (malate, citrate) or no agreement (GABA, aspartate) with the measured values. Error bars for the measured data represent 90% confidence intervals of metabolite levels at the developmental time points of interest, estimated using the curve-fitting approach described by Colombié *et al.* (2015). Error bars on predicted data represent the ranges of possible flux values predicted using flux variability analysis (FVA).

GrOE-FBA: insights into tomato fruit development

Two major biological insights emerged from the analysis of the GrOE-FBA model of tomato fruit development. First, we demonstrate that transitory carbohydrate stores are only predicted by the model if a constraint is added that gradually decreases the rate of influx of nutrients from the phloem. Our model demonstrates that because of the decline in phloem influx during development, the accumulation of starch (or other carbohydrates such as sucrose) in the earlier stages of fruit development is required to meet the carbon demand in later stages. The question then arises as to why the phloem influx into a fruit declines below the level required to maintain its metabolic requirements. One possibility is that because of the staggered initiation of fruits along a truss, it is necessary to progressively reduce the share of phloem nutrients taken by maturing fruit to allow younger fruits, which have lower sink strength, to develop successfully. Temporal extension

of starch synthesis has been reported to result in increased fruit size (Petreikov *et al.*, 2006, 2009). This is in agreement with our hypothesis. Increased sucrose demand owing to starch synthesis will increase the sink strength of smaller fruits. Once the fruits are bigger, the greater transitory starch stores will reduce their sink strength, resulting in more phloem constituents being available to the smaller fruits.

The second biological insight is the relatively minor impact biomass demand had on developing fruit metabolism (Figure 5). It is known that cell expansion results in an increase in cell wall and cell membrane content. The protein content of cells is also thought to increase in order to maintain the optimal concentration required for unhampered metabolism. In most FBA models of growing plant tissues published to date, the synthesis of these biomass components is the main drain on the metabolic system. The GrOE-FBA model demonstrates that for tissues growing by the expansion of existing cells, the demand for these biomass elements imposes only a small fraction of the metabolic cost. Instead, the dominant demand on metabolism was solute accumulation for osmotically driven cell expansion. The accumulation of solutes was responsible for most of the gain in fruit DW from 18.0 to 43.7 DPA (Table 1). From this we can conclude that the drivers for metabolism in expanding cells are significantly different from those in dividing cells, and that osmolarity-based constraints such as GrOE-FBA applied in this study are necessary to model metabolism in tissues growing by cell expansion.

GrOE-FBA: limitations of the approach

GrOE-FBA is a modified form of FBA and hence inherits its limitations (Sweetlove and Ratcliffe, 2011), including not being able to predict futile cycles. A substantial fraction of the energy consumption in a tomato cell suspension has been attributed to the operation of such cycles (Rontein *et al.*, 2002) and the FBA model is unable to capture this energy expenditure. Although this might explain the discrepancy between the glucose consumption rate of the model ($3.57 \text{ mg ml}^{-1} \text{ day}^{-1}$) and the value reported in the literature (glucose influx rate for day 4 is $5.34 \text{ mg ml}^{-1} \text{ day}^{-1}$), it should also be noted that the method used to estimate the futile cycles has been questioned because of the complicating effects of the subcellular structure of the metabolic network (Kruger *et al.*, 2007).

Another limitation of GrOE-FBA is that it focuses on the osmotic significance of the accumulating solutes and makes no attempt to tackle the challenges involved in imposing constraints on metabolism related to insect resistance, texture and flavour. Nevertheless, introducing such constraints into the model might improve its ability to predict sucrose and organic acid levels.

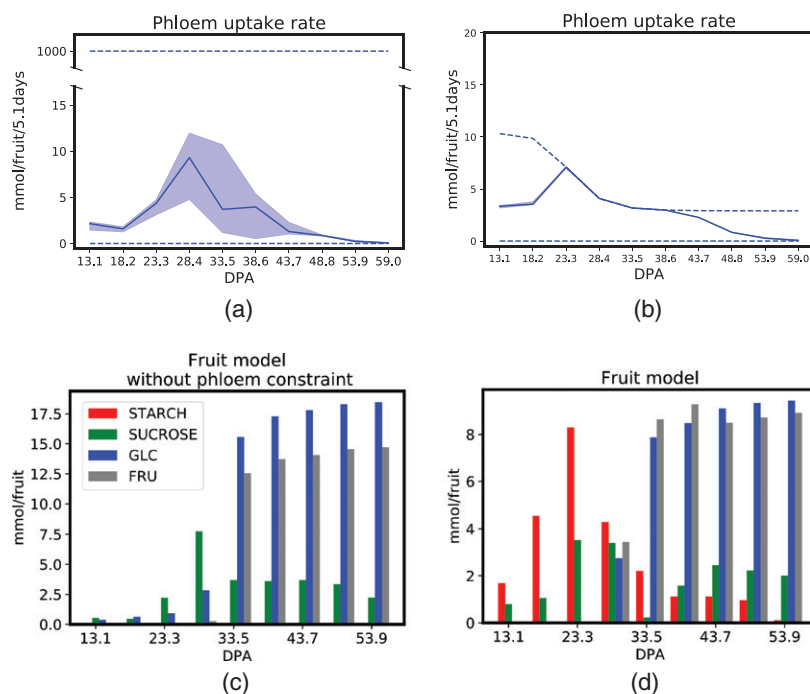


Figure 7. Impact of phloem uptake rate on the need for a transitory carbohydrate store during *Solanum lycopersicum* (tomato) fruit development. The multi-phase growth-by-osmotic-expansion flux balance analysis (GrOE-FBA) model was run with the phloem uptake rate either effectively unconstrained (allowing the model to choose a rate between 0 and 1000 mmol per fruit per 5.1 days) (a) or constrained with the upper bound based on the measurements of Walker and Ho (1977a,b) (b). The upper and lower bounds of the phloem uptake rate are plotted as dotted lines, and the optimal value chosen by the model is plotted as a solid line, together with the flux variability analysis (FVA) range for the solution (shaded). Applying the upper bound to the phloem uptake rate creates a carbon and/or energy limitation in phases 4 and 5 (28.4–33.5 DPA) of the multiphase fruit model. The predicted starch and soluble sugar contents obtained with the phloem uptake rate either unconstrained (c) or constrained (d) show that phloem uptake rate constraints are responsible for the temporary carbohydrate build-up observed in the early stages of fruit development.

Finally, the GrOE-FBA model predicts metabolic fluxes by flux optimization and does not account for signalling and the regulation of metabolism, although these could be included in the form of experimental constraints on maximal enzyme activity. As a result, the model we present does not activate flux through energy dissipation mechanisms (such as alternative NADH dehydrogenases and alternative oxidase), and hence the GrOE-FBA model is unable to predict the respiratory climacteric (Colombié *et al.*, 2017). A computationally expensive FBA approach termed cost-weighted flux minimization has been shown to be capable of predicting alternative pathways in source leaves (Cheung *et al.*, 2015). Such an approach might allow the multiphase GrOE-FBA tomato model to predict metabolically inefficient processes, such as uncoupled respiration and futile cycles.

CONCLUSION

GrOE-FBA, an FBA approach that uses volume-based osmotic constraints, allows metabolism to be modelled during cell expansion, and thus extends the scope of constraints-based metabolic modelling to growing tissues in which the expansion of existing cells is the dominant driver of growth. Understanding metabolism in expanding

cells could help develop engineering strategies to optimize metabolism during the cell expansion phase of leaf and root development. The approach could also be used to study metabolism in guard cells where turgor-pressure-driven changes in cell size regulate stomatal aperture, in turn determining CO₂ assimilation and transpiration rates. GrOE-FBA could therefore help complement current kinetic models of guard cells (Hills *et al.*, 2012) with a more holistic modelling approach. Recently, there has been increased interest in combining metabolic models with whole-plant developmental models (Marshall-Colon *et al.*, 2017). Using GrOE-FBA to account for the metabolism of expanding cells could help to improve the relevance of the metabolic models in the context of whole-plant growth and potentially improve the predictive power of integrated metabolic whole-plant growth models.

EXPERIMENTAL PROCEDURES

Plant material and growth conditions

Tomato (*S. lycopersicum* cv. 'Moneymaker') seeds were sterilized and germinated on Murashige-Skoog (MS) medium. The plants were grown in a glasshouse with a 16-h photoperiod (22–23°C day; 20–22°C night) and with supplementary lighting to maintain an irradiance of 250–400 $\mu\text{mol m}^{-2} \text{sec}^{-1}$. Lateral stems were

systematically removed. Each flower anthesis was recorded, and trusses were pruned at five developed fruits to limit fruit size heterogeneity. Tomato fruits were harvested at nine different developmental stages corresponding to 8, 15, 22, 28, 34, 42, 50, 52 and 59 DPA, with the last four corresponding to mature green, turning, orange and red fruit developmental stages, respectively. Fruit samples were collected from the first two levels of trusses in the plant. All materials were frozen in liquid nitrogen and storage at -80°C until use.

Fruit biomass measurements and morphology analysis

Cell wall was extracted according to an established protocol (Ruprecht *et al.*, 2011). The remaining insoluble material was washed with water and ethanol, air dried and weighed. Lipids were extracted from a known mass of ground tissue using the chloroform/methanol protocol (Bligh and Dyer, 1959). Protein, extracted with 6 M urea, 2 M thiourea buffer (Salem *et al.*, 2016), was quantified using the Bradford assay (Bradford, 1976). The amino acid content of protein hydrolysates (50% w/v trichloroacetic acid, 6 M HCl, $100^{\circ}\text{C}/24\text{ h}$) (Antoniewicz *et al.*, 2007) was determined by an established gas chromatography (GC)/electron impact time-of-flight mass spectroscopy (EI-TOF-MS) protocol (Luedemann *et al.*, 2008; Fernie *et al.*, 2011; Osorio *et al.*, 2011). Starch content was determined by enzymatic digestion and spectrophotometric assay of the resultant glucose (Hendriks *et al.*, 2003). Fruit height and diameter were measured using a calibrated digital vernier. The fresh weight to dry weight ratio (FW/DW) was determined by weighing fresh tissues and reweighing them after drying to constant weight in a forced-air oven at 65°C .

Gas chromatography mass spectrometry of fruit content

Metabolite analysis of fruit samples was performed using GC/EI-TOF-MS (Lisec *et al.*, 2006). Plant material was extracted using a method described elsewhere (Osorio *et al.*, 2011). Data analysis was performed using CHROMATOF 1.0 (Leco, <https://www.leco.com>) and TAGFINDER 4.0 (Luedemann *et al.*, 2008). Cross-referencing of mass spectra was performed with the Golm Metabolome database (Kopka *et al.*, 2005). Documentation of metabolite profiling data acquisition is reported following recommended guidelines (Fernie *et al.*, 2011). Curve fitting (Colombié *et al.*, 2015) was used to generate curves for metabolite content and fluxes based on experimental measurements.

Flux balance analysis and flux variability analysis

Metabolic reactions associated with phospholipid biosynthesis (PC, PE and PA), amino acid catabolism, nucleotide biosynthesis, β oxidation, lycopene biosynthesis and phytol metabolism were added to a previously published mass and charge-balanced model of primary metabolism in plant cells (Shameer *et al.*, 2018) to generate the model PlantCoreMetabolism_v1_2. A complete log of all model curations and associated literature is presented in Table S2. Parsimonious FBA (pFBA) and flux variability analysis (FVA) functions available in COBRAPY 0.13.4 (Ebrahim *et al.*, 2013) were updated to perform weighted pFBA and weighted FVA, respectively. Aggregator reactions used to measure fruit metabolite content were given a zero weighting, whereas all other reactions were given a weight of 1. COBRAPY in JUPYTER NOTEBOOK (PYTHON 2.7) was used to run and document all scripts. BINDER was used to generate interactive versions of the JUPYTER NOTEBOOKS used in the study. All scripts, data, models, associated files and the link to launch BINDER have been made available in a Github repository (<https://github.com/ljs1002/Shameer-et-al-Predicting-metabolism-during-growth-by-osmotic-cell-expansion>).

Estimating maintenance costs

Non-growth associated maintenance (NGAM) costs in all models were represented by flux through an ATPase and three NADPH oxidase (cytosolic, mitochondrial and plastidic) pseudo-reactions, constrained to a 3:1 (ATP hydrolysis:NADPH oxidase) ratio based on the results of a previously published study (Cheung *et al.*, 2013).

Dividing cells were assumed to have a carbon conversion efficiency (CCE) of 70% based on measurements for a range of plant tissues and species (Chen and Shachar-Hill, 2012). Fluxes through the NGAM reactions in the dividing cell model were gradually increased until a CCE of approximately 70% was achieved. When the NGAM ATPase flux was constrained to $0.062\text{ mmol ml}^{-1}\text{ day}^{-1}$, the CCE of the system was observed to be 69.92%. This NGAM ATPase flux was then used to constrain maintenance in the dividing cell model. The same NGAM constraints were imposed on the expanding cell model.

Each phase of the multiphase GroE-FBA model was 5.1 days long. The mean respiratory cost of NGAM based on data reported by Walker and Thornley (1977) was assumed to be 1.7 mmol CO_2 per fruit per day throughout fruit development. Note that these results indicated that the maintenance costs per unit mass of fruit decreased during fruit growth, leading to an approximately constant maintenance cost per fruit. This is equivalent to 8.5 mmol CO_2 per fruit per 5.1 days. Using a model of primary metabolism in pericarp cell constrained so as to prevent the net synthesis of any metabolite, an NGAM ATPase flux of 26.2 mmol CO_2 per fruit per 5.1 days was found to result in a respiration rate of 8.5 mmol CO_2 per fruit per 5.1 days. This NGAM ATPase flux was used to constrain NGAM in all phases of fruit development.

Modelling primary metabolism in a dividing heterotrophic cell suspension

The PlantCoreMetabolism_v1_2 model was used to generate representations of metabolism in dividing tomato cells. Previously published data from tomato heterotrophic cell suspension cultures report a maximum growth rate of $2\text{ mg DW ml}^{-1}\text{ day}^{-1}$ (Rontein *et al.*, 2002). Data on the biomass content (cell wall, sugars, organic acids and proteins) of cells demonstrating the maximum growth rate, from the same study, was used to generate a biomass equation for the dividing cell system as in conventional FBA modelling. The lipid:cellulose content ratio reported in Arabidopsis cell cultures (Williams *et al.*, 2010) was used to estimate the lipid content of the cells and the biomass equation was updated accordingly. The biomass accumulation rate of the model was constrained to $2\text{ mg DW ml}^{-1}\text{ day}^{-1}$. For the sake of simplification, the cell wall and cell membrane were assumed to be composed of only cellulose and PA, respectively. Constraints based on Equation 2 were introduced to promote solute partitioning between the cytosol and the vacuole. With the lack of data available for heterotrophic tomato cells, the value for V_v/V_c required for Equation 2 was calculated from data published on tomato pericarp subcellular volume fractions (Beauvoit *et al.*, 2014). NGAM was represented in the model as described earlier. Glucose was set as the sole carbon source and FBA, with the minimization of the sum of fluxes as the objective, was used to predict the optimal flux distribution.

Modelling primary metabolism in a system of expanding 26-DPA pericarp cells

The PlantCoreMetabolism_v1_2 model was used to generate representations of metabolism in expanding 26-DPA tomato

pericarp cells. The rate of cell expansion was estimated to be at its highest in 26-DPA tomato pericarp cells ($0.174 \text{ nl cell}^{-1} \text{ day}^{-1}$; estimated from data in Beauvoit *et al.*, 2014). For the sake of consistency, the number of cells in the expanding cell system was kept equal to that in the dividing cell suspension when the growth rate attained the maximum rate of $2 \text{ mg DW ml}^{-1} \text{ day}^{-1}$ ($1.45 \times 10^6 \text{ cells ml}^{-1}$). The composition of soluble metabolites in 26-DPA pericarp cells were estimated from third-degree polynomial curves fitted to published experimental data (Colombié *et al.*, 2015). Equations 1 and 2 were used to introduce osmotic constraints in the model and the values for V_{cell} and C_{cell} were estimated from published data (Almeida and Huber, 1999; Beauvoit *et al.*, 2014). The difference in osmotic content between DPA 26 and 27 was used to set the demand for osmolytes. Data on subcellular volume fractions published by Beauvoit *et al.* were used to calculate $V_{\text{c}}/V_{\text{c}}$ at 26 DPA. The difference between cellulose, lipid and protein contents between DPA 26 and 27, as calculated from Equations 3–5, was used to set the demand for these biomass elements. NGAM was represented in the model as described earlier. Uptake of sucrose and amino acids from the phloem was permitted and FBA was used to predict metabolic fluxes that minimized the sum of fluxes while maximizing the organic content.

Implementation of GrOE-FBA constraints in the multiphase developing fruit model

Tomato fruit development from 13.1 to 43.7 DPA (mature green fruits observed at 42 DPA) is mainly the result of the expansion of existing cells (Gillaspy *et al.*, 1993) and GrOE-FBA was used to model metabolism during these stages. The model extended to 54 DPA to allow the final metabolite composition of ripe fruit to be incorporated as a constraint. Assuming the tomato fruit is composed of uniformly packed pericarp cells, Equation 1 can be transformed to the following form for a whole fruit:

$$\sum n_i m_i = C_{\text{cell}} V_{\text{fruit}}, \quad (6)$$

where i is a metabolite/ion in the fruit and V_{fruit} is the volume of the fruit.

Constraints based on Equations 2 and 6 were imposed on each phase of the multiphase developing fruit model. Previously published data on subcellular volume fractions (Beauvoit *et al.*, 2014) were used to calculate $V_{\text{c}}/V_{\text{c}}$ during the different stages of fruit development and C_{cell} was estimated based on osmolalities reported in the literature (Almeida and Huber, 1999). Values for V_{fruit} for all 10 phases of fruit development modelled were determined experimentally (Table S1).

The pericarp cell volume for each phase of the multiphase fruit model was calculated from published data (Beauvoit *et al.*, 2014), and cellulose, phospholipid and protein demand fluxes were imposed on the system using Equations 3–5, scaling them from $\mu\text{mol per cell}$ to mmol per fruit .

The carbon influx rate into developing tomato fruits has been reported to be inversely proportional to fruit carbon content and size (Walker and Ho, 1977a,b). A hyperbolic curve was fitted to capture the relationship between carbon influx rates and fruit carbon content more accurately. Fruit carbon content has been reported to be linearly related to fruit volume (Walker and Ho, 1997b). Hence, the initial carbon content for each developmental phase was calculated based on fruit volume at the respective phases. These values were then used to predict the upper bounds for the flux of nutrients from the phloem in the respective phases of the developing tomato model.

ACKNOWLEDGEMENTS

Funding from the European Research Area Network for Coordinating Action in Plant Sciences (ERA-CAPS) ('Simultaneous manipulation of source and sink metabolism for improved crop yield'; BO 1482/18-1 | FE 552/33-1 | RE 1351/2-1 | SW 122/2-1) is acknowledged.

AUTHOR CONTRIBUTIONS

SS, RGR and LJS developed the GrOE-FBA framework; ARF, RGR and LJS designed the experiments and supervised the study; JGV collected and analysed all biological data; SS performed the modelling and analysed the results; SS, JGV, RGR and LJS wrote the article; all authors approved the final version of the article for publication.

CONFLICT OF INTEREST

There are no conflicts of interest.

DATA AVAILABILITY STATEMENT

All computational code required to reproduce this study is available from the following Github repository: <https://github.com/ljs1002/Shameer-et-al-Predicting-metabolism-during-growth-by-osmotic-cell-expansion>. All other data generated and used in this study are available from the supporting information.

SUPPORTING INFORMATION

Additional Supporting Information may be found in the online version of this article.

Figure S1. Expanding cells show higher ATP demand associated with solute accumulation when compared with dividing cells, irrespective of the non-growth associated maintenance (NGAM) ATP hydrolysis and NADPH oxidase flux ratio constraints.

Figure S2. Comparison of predicted and measured metabolite contents in developing tomato fruit.

Table S1. List of parameters used in the study.

Table S2. Model curation log for the PlantCoreMetabolism_v1_2 model.

Appendix S1. Derivations for Equations 1–5.

Appendix S2. Tomato fruit fresh weight, fresh weight/dry weight ratio, organic solute content, starch content, protein content, cell wall content and lipid content during different stages of fruit development.

Appendix S3. Predicted metabolic fluxes in dividing cell, expanding cell and developing fruit models.

Appendix S4. Systems Biology Markup Language (SBML) version of the fully constrained multiphase developing tomato model.

REFERENCES

- Almeida, D.P.F. and Huber, D.J. (1999) Apoplastic pH and inorganic ion levels in tomato fruit: a potential means for regulation of cell wall metabolism during ripening. *Physiol. Plant.* **105**, 506–512.
- Antoniewicz, M.R., Kelleher, J.K. and Stephanopoulos, G. (2007) Accurate assessment of amino acid mass isotopomer distributions for metabolic flux analysis. *Anal. Chem.* **79**, 7554–7559.
- Beauvoit, B.P., Colombié, S., Monier, A. *et al.* (2014) Model-assisted analysis of sugar metabolism throughout tomato fruit development reveals

- enzyme and carrier properties in relation to vacuole expansion. *Plant Cell*, **26**, 3224–3242.
- Biais, B., Bénard, C., Beauvoit, B. *et al.* (2014) Remarkable reproducibility of enzyme activity profiles in tomato fruits grown under contrasting environments provides a roadmap for studies of fruit metabolism. *Plant Physiol.* **164**, 1204–1221.
- Bligh, E.G. and Dyer, W.J. (1959) A rapid method of total lipid extraction and purification. *Can. J. Biochem. Physiol.* **37**, 911–917.
- Boyer, J.S., Cavalieri, A.J. and Schulze, E.-D. (1985) Control of the rate of cell enlargement: Excision, wall relaxation, and growth-induced water potentials. *Planta*, **163**, 527–543.
- Bradford, M.M. (1976) A rapid and sensitive method for the quantitation of microgram quantities of protein utilizing the principle of protein-dye binding. *Anal. Biochem.* **72**, 248–254.
- Cacas, J.-L., Buré, C., Grosjean, K. *et al.* (2016) Revisiting plant plasma membrane lipids in tobacco: a focus on sphingolipids. *Plant Physiol.* **170**, 367–384.
- Carrari, F. and Fernie, A.R. (2006) Metabolic regulation underlying tomato fruit development. *J. Exp. Bot.* **57**, 1883–1897.
- Carrari, F., Baxter, C., Usadel, B. *et al.* (2006) Integrated analysis of metabolite and transcript levels reveals the metabolic shifts that underlie tomato fruit development and highlight regulatory aspects of metabolic network behavior. *Plant Physiol.* **142**, 1380–1396.
- Chen, X. and Shachar-Hill, Y. (2012) Insights into metabolic efficiency from flux analysis. *J. Exp. Bot.* **63**, 2343–2351.
- Cheung, C.Y.M., Williams, T.C.R., Poolman, M.G., Fell, D.A., Ratcliffe, R.G. and Sweetlove, L.J. (2013) A method for accounting for maintenance costs in flux balance analysis improves the prediction of plant cell metabolic phenotypes under stress conditions. *Plant J.* **75**, 1050–1061.
- Cheung, C.Y.M., Poolman, M.G., Fell, D.A., Ratcliffe, R.G. and Sweetlove, L.J. (2014) A diel flux balance model captures interactions between light and dark metabolism during day-night cycles in *C₃* and crassulacean acid metabolism leaves. *Plant Physiol.* **165**, 917–929.
- Cheung, C.Y.M., Ratcliffe, R.G. and Sweetlove, L.J. (2015) A method of accounting for enzyme costs in flux balance analysis reveals alternative pathways and metabolite stores in an illuminated Arabidopsis leaf. *Plant Physiol.* **169**, 1671–1682.
- Cohen, S., Itkin, M., Yeselson, Y. *et al.* (2014) The *PH* gene determines fruit acidity and contributes to the evolution of sweet melons. *Nat. Commun.* **5**, 4026.
- Colombié, S., Nazaret, C., Bénard, C. *et al.* (2015) Modelling central metabolic fluxes by constraint-based optimization reveals metabolic reprogramming of developing *Solanum lycopersicum* (tomato) fruit. *Plant J.* **81**, 24–39.
- Colombié, S., Beauvoit, B., Nazaret, C. *et al.* (2017) Respiration climacteric in tomato fruits elucidated by constraint-based modelling. *New Phytol.* **213**, 1726–1739.
- Ebrahim, A., Lerman, J.A., Pálsson, B.O. and Hyduke, D.R. (2013) COBRApy: constraints-based reconstruction and analysis for python. *BMC Syst. Biol.* **7**, 74.
- Fahlgren, N., Gehan, M.A. and Baxter, I. (2015) Lights, camera, action: high-throughput plant phenotyping is ready for a close-up. *Curr. Opin. Plant Biol.* **24**, 93–99.
- Feist, A.M. and Pálsson, B.O. (2010) The biomass objective function. *Curr. Opin. Microbiol.* **13**, 344–349.
- Feist, A.M., Henry, C.S., Reed, J.L., Krummenacker, M., Joyce, A.R., Karp, P.D., Broadbelt, L.J., Hatzimanikatis, V. and Pálsson, B.O. (2007) A genome-scale metabolic reconstruction for *Escherichia coli* K-12 MG1655 that accounts for 1260 ORFs and thermodynamic information. *Mol. Syst. Biol.* **3**, 121.
- Fernie, A.R., Aharoni, A., Willmitzer, L., Stitt, M., Tohge, T., Kopka, J., Carroll, A.J., Saito, K., Fraser, P.D. and DeLuca, V. (2011) Recommendations for reporting metabolite data. *Plant Cell*, **23**, 2477–2482.
- Gillaspy, G., Ben-David, H. and Gruissem, W. (1993) Fruits: a developmental perspective. *Plant Cell*, **5**, 1439–1451.
- Gomes de Oliveira Dal'Molin, C. and Nielsen, L.K. (2018) Plant genome-scale reconstruction: from single cell to multi-tissue modelling and omics analyses. *Curr. Opin. Biotechnol.* **49**, 42–48.
- Gomes de Oliveira Dal'Molin, C., Quek, L.-E., Saa, P.A. and Nielsen, L.K. (2015) A multi-tissue genome-scale metabolic modeling framework for the analysis of whole plant systems. *Front. Plant Sci.* **6**, 4.
- Gonzalez, N., Vanhaeren, H. and Inzé, D. (2012) Leaf size control: complex coordination of cell division and expansion. *Trends Plant Sci.* **17**, 332–340.
- Grafahrend-Belau, E., Junker, A., Eschenroder, A., Müller, J., Schreiber, F. and Junker, B.H. (2013) Multiscale metabolic modeling: Dynamic flux balance analysis on a whole-plant scale. *Plant Physiol.* **163**, 637–647.
- Guclu, J., Paulin, A. and Soudain, P. (1989) Changes in polar lipids during ripening and senescence of cherry tomato (*Lycopersicon esculentum*): relation to climacteric and ethylene increases. *Physiol. Plant.* **77**, 413–419.
- Hendriks, J.H.M., Kolbe, A., Gibon, Y., Stitt, M. and Geigenberger, P. (2003) ADP-glucose pyrophosphorylase is activated by posttranslational redox-modification in response to light and to sugars in leaves of Arabidopsis and other plant species. *Plant Physiol.* **133**, 838–849.
- Hills, A., Chen, Z.-H., Amtmann, A., Blatt, M.R. and Lew, V.L. (2012) OnGuard, a computational platform for quantitative kinetic modeling of guard cell physiology. *Plant Physiol.* **159**, 1026–1042.
- Ho, L.C. and Hewitt, J.D. (1986) Fruit development. In *The Tomato Crop A scientific basis for improvement* (Antherton, J. and Rudich, J. eds). London: Chapman and Hall, pp. 201–240.
- Kopka, J., Schauer, N., Krueger, S. *et al.* (2005) GMD@CSB.DB: the Golm metabolome database. *Bioinformatics*, **21**, 1635–1638.
- Kruger, N.J., Le Lay, P. and Ratcliffe, R.G. (2007) Vacuolar compartmentation complicates the steady-state analysis of glucose metabolism and forces reappraisal of sucrose cycling in plants. *Phytochemistry*, **68**, 2189–2196.
- Legland, D., Devaux, M.F., Bouchet, B., Guillon, F. and Lahaye, M. (2012) Cartography of cell morphology in tomato pericarp at the fruit scale. *J. Microsc.* **247**, 78–93.
- Lisec, J., Schauer, N., Kopka, J., Willmitzer, L. and Fernie, A.R. (2006) Gas chromatography mass spectrometry-based metabolite profiling in plants. *Nat. Protoc.* **1**, 387–396.
- Luedemann, A., Strassburg, K., Erban, A. and Kopka, J. (2008) TagFinder for the quantitative analysis of gas chromatography - mass spectrometry (GC-MS)-based metabolite profiling experiments. *Bioinformatics*, **24**, 732–737.
- Lynch, J.P. (2019) Root phenotypes for improved nutrient capture: an under-exploited opportunity for global agriculture. *New Phytol.* **223**, 548–564.
- Marshall-Colon, A., Long, S.P., Allen, D.K. *et al.* (2017) Crops *In Silico*: generating virtual crops using an integrative and multi-scale modeling platform. *Front. Plant Sci.* **8**, 786.
- Nikoloski, Z., Perez-Storey, R. and Sweetlove, L.J. (2015) Inference and prediction of metabolic network fluxes. *Plant Physiol.* **169**, 1443–1455.
- Osorio, S., Do, P.T. and Fernie, A.R. (2011) Profiling primary metabolites of tomato fruit with gas chromatography/mass spectrometry. In *Plant Metabolomics. Methods in Molecular Biology (Methods and Protocols)* (Hardy, N.W. and Hall, R.D. eds). New York: Humana Press, pp. 101–109.
- Petreikov, M., Shen, S., Yeselson, Y., Levin, I., Bar, M. and Schaffer, A.A. (2006) Temporally extended gene expression of the ADP-Glc pyrophosphorylase large subunit (AgpL1) leads to increased enzyme activity in developing tomato fruit. *Planta*, **224**, 1465–1479.
- Petreikov, M., Yeselson, L., Shen, S., Levin, I., Schaffer, A.A., Dagan, B., Efrati, A., Bar, M. and Co, G.S. (2009) Carbohydrate balance and accumulation during development of near-isogenic tomato lines differing in the AGPase-L1 allele. *J. Am. Soc. Hortic. Sci.* **134**, 134–140.
- Rolin, D., Baldet, P., Just, D., Chevalier, C., Biran, M. and Raymond, P. (2000) NMR study of low subcellular pH during the development of cherry tomato fruit. *Aust. J. Plant Physiol.* **27**, 61–69.
- Rontein, D., Dieuaide-Noubhani, M., Dufourc, E.J., Raymond, P. and Rolin, D. (2002) The metabolic architecture of plant cells. *J. Biol. Chem.* **277**, 43948–43960.
- Ruprecht, C., Mutwil, M., Saxe, F., Eder, M., Nikoloski, Z. and Persson, S. (2011) Large-scale co-expression approach to dissect secondary cell wall formation across plant species. *Front. Plant Sci.* **2**, 23.
- Salem, M.A., Jüppner, J., Bajdzienko, K. and Gialvalisco, P. (2016) Protocol: a fast, comprehensive and reproducible one-step extraction method for the rapid preparation of polar and semi-polar metabolites, lipids, proteins, starch and cell wall polymers from a single sample. *Plant Methods*, **12**, 45.

- Scheunemann, M., Brady, S.M. and Nikoloski, Z. (2018) Integration of large-scale data for extraction of integrated Arabidopsis root cell-type specific models. *Sci. Rep.* **8**, 7919.
- Schwender, J. and Hay, J.O. (2012) Predictive modeling of biomass component tradeoffs in brassica napus developing oilseeds based on *in silico* manipulation of storage metabolism. *Plant Physiol.* **160**, 1218–1236.
- Shameer, S., Baghalian, K., Cheung, C.Y.M., Ratcliffe, R.G. and Sweetlove, L.J. (2018) Computational analysis of the productivity potential of CAM. *Nat. Plants*, **4**, 165–171.
- Shaw, R. and Cheung, C.Y.M. (2018) A dynamic multi-tissue flux balance model captures carbon and nitrogen metabolism and optimal resource partitioning during Arabidopsis growth. *Front. Plant Sci.* **9**, 884.
- Sweetlove, L.J. and Ratcliffe, R.G. (2011) Flux-balance modeling of plant metabolism. *Front. Plant Sci.* **2**, 38.
- Taiz, L. (1992) The plant vacuole. *J. Exp. Biol.* **172**, 113–122.
- Takayama, M. and Ezura, H. (2015) How and why does tomato accumulate a large amount of GABA in the fruit? *Front. Plant Sci.* **6**, 612.
- Tardieu, F., Cabrera-Bosquet, L., Pridmore, T. and Bennett, M. (2017) Plant phenomics, from sensors to knowledge. *Curr. Biol.* **27**, R770–R783.
- Tohge, T., Alseekh, S. and Fernie, A.R. (2014) On the regulation and function of secondary metabolism during fruit development and ripening. *J. Exp. Bot.* **65**, 4599–4611.
- Valle, E.M., Boggio, S.B. and Heldt, H.W. (1998) Free amino acid composition of phloem sap and growing fruit of *Lycopersicon esculentum*. *Plant Cell Physiol.* **39**, 458–461.
- Varma, A. and Palsson, B.O. (1994) Stoichiometric flux balance models quantitatively predict growth and metabolic by-product secretion in wild-type *Escherichia coli* W3110. *Appl. Environ. Microbiol.* **60**, 3724–3731.
- Walker, A.J. and Ho, L.C. (1977a) Carbon translocation in the tomato: carbon import and fruit growth. *Ann. Bot.* **41**, 813–823.
- Walker, A.J. and Ho, L.C. (1977b) Carbon translocation in the tomato: effects of fruit temperature on carbon metabolism and the rate of translocation. *Ann. Bot.* **41**, 825–832.
- Walker, A.J. and Thornley, J.H.M. (1977) The tomato fruit: Import, growth, respiration and carbon metabolism at different fruit sizes and temperatures. *Ann. Bot.* **41**(1976), 977–985.
- Williams, T.C.R., Poolman, M.G., Howden, A.J.M., Schwarzlander, M., Fell, D.A., Ratcliffe, R.G. and Sweetlove, L.J. (2010) A genome-scale metabolic model accurately predicts fluxes in central carbon metabolism under stress conditions. *Plant Physiol.* **154**, 311–323.
- Yuan, H., Cheung, C.Y.M., Poolman, M.G., Hilbers, P.A.J. and van Riel, N.A.W. (2016) A genome-scale metabolic network reconstruction of tomato (*Solanum lycopersicum* L.) and its application to photorespiratory metabolism. *Plant J.* **85**, 289–304.